Molecular Crystals and Liquid Crystals

ISSN: (Print) (Online) Journal homepage: https://www.tandfonline.com/loi/gmcl20

Optical absorption in core-shell quantum antidot under applied co-directed electric and magnetic fields

V. A. Holovatsky & M. V. Chubrei

To cite this article: V. A. Holovatsky & M. V. Chubrei (2022): Optical absorption in core-shell quantum antidot under applied co-directed electric and magnetic fields, Molecular Crystals and Liquid Crystals, DOI: 10.1080/15421406.2022.2073539

To link to this article: https://doi.org/10.1080/15421406.2022.2073539

Published online: 13 May 2022.

MOLECULAR CRYSTALS AND LIQUID CRYSTALS
https://doi.org/10.1080/15421406.2022.2073539

Taylor & Francis
Taylor & Francis Group

Optical absorption in core-shell quantum antidot under applied co-directed electric and magnetic fields

V. A. Holovatsky and M. V. Chubrei

Department of Theoretical Physics and Computer Simulation, Yuriy Fedkovych Chernivtsi National University, Chernivtsi, Ukraine

ABSTRACT

Using the matrix diagonalization method within the effective mass approximation and the rectangular potential profile, we investigate optical absorption coefficients (OAC) in the core-shell quantum antidot (QAD) $Al_{0.3}Ga_{0.7}As/GaAs/Al_{0.3}Ga_{0.7}As$ in the presence of applied co-directed electrical and magnetic fields. The electric field effect on the electron wave functions, energy spectrum, oscillator strength of the intersubband electronic transitions is calculated for different size of QAD core and different value of the magnetic field induction. The total, linear and nonlinear optical absorption coefficients in QAD are obtained by considering 1 s-1p and 1p-1d electron quantum transitions as functions of the incident photon energy.

KEYWORDS

density distribution; energy spectrum; intersubband transition; optical absorption coefficient; quantum antidot

Introduction

Multilayer spherical quantum dots (MSQD) have attracted much of scientists' attention due to modern technology of their growth and wide range of their application in electronic and optoelectronic devices. One of the most famous MSQD is so-called inverted core-shell QD (core-shell antidot), which consists of a core and a shell (a core has a wider bandgap than a shell). Based on the core-shell QD numbers of biosensors, fluorescent labels, light-emitting devices and solar cells have already been created, and elements for modern computer technology are being developed [1–6]. Some products still function as prototypes, some are partially implemented somewhere, and some have already been in use practically. The creation of new optoelectronic and magneto-optical semiconductor devices requires the study of an external electric or magnetic field influence on the energy spectrum and wave functions of quasiparticles at quantum dots. Such studies have been performed by many scientists and by different methods for various spherical quantum dots [7–18].

The researchers [7–9] obtain the ground and first excited states energy eigenvalues and eigenfunctions of an electron confined in nanosystem in the presence of external electric and magnetic field using the standard iterative numerical method. This study shows that the absorption coefficient peak values decrease with the electric field

CONTACT V. Holovatsky v.holovatsky@chnu.edu.ua Department of Theoretical Physics and Computer Simulation, Yuriy Fedkovych Chernivtsi National University, 2, Kotsyubynsky Str., 58002 Chernivtsi, Ukraine

increase. The magnetic field shifts the intersubband transition energies to the high-energy region.

V. Harutyunyan [10] obtained the wave functions and energy spectrum of single-particle states in the nanospherical heterolayer structure in the presence of an external electrical field in an explicit form using the adiabatic approximation. Perturbative, WKB and variation approach [11] have been used to study effect of the radial electrostatic field different value on intersubband transition in a spherical nanolayer.

Most studies of the electric and magnetic fields influence on the energy spectrum and optical properties of spherical quantum dots are performed by the matrix diagonalization method [15–25]. This method can be used to obtain eigenvalues and eigenfunctions of the Hamiltonian with perturbations that break the spherical symmetry of the problem. Different studies use various orthonormal bases to expand the wave function. For example, Çakır *et al.* used the linear combination of Slater type orbitals [15–16], Stevanović *et al.* used the variational Lagrange mesh method with functions constructed from the shifted Legendre polynomials [17,18]. Many scientists used the matrix method with orthonormal basis of functions, which are exact solutions of the corresponding spherically symmetric problem [19–27]. The high accuracy of the results obtained by this method is confirmed by comparison with the numerical solutions of the Schrödinger equation obtained by the finite element method [25].

The studies of the electric and magnetic fields simultaneous influence on the linear and nonlinear intersubband optical properties concerned QD with parabolic confined potential [7–9, 13] and MSQD with impurity [22]. The results of the last-mentioned study confirmed the significant influence of electric and magnetic fields on the optical rectification coefficient, the second-order and third harmonic generations spectra in MSQD.

Kassapoglu *et al.* used the matrix diagonalization method investigating the effect of an externally applied magnetic field on the energy states 1 s, 1p, 1d and 1f in the spherical quantum dot with finite and infinite confinement potentials [27]. The energies of the allowed transitions and related OAC were calculated and analyzed. Researchers report that the magnetic field shifts the total OAC peaks related to $\sigma+$ and $\sigma-$ transitions (circular polarized light absorption) and unaffected by the magnetic field on the absorption peak related to π-polarized light.

As far as we know, a detailed theoretical study of the total OAC in the presence of external magnetic and electric fields on a spherical MSQD has not been sufficiently studied, although, in our opinion, some investigation in this area is important for the development of new devices. In this study the effect of the codirected electrical and magnetic fields on the electron energy spectrum, wave functions, oscillator strengths of the intersubband quantum transitions and optical absorption coefficient corresponding to the transitions 1 s-1p, 1p-1d and 1d-1f for QAD with different core radii are investigated.

The calculations have been made in the framework of the effective mass approximation via the matrix diagonalization method by using the complete basis of electron wave functions in the absence of the electric and magnetic field [19, 25]. The OACs associated with allowed transition are calculated using the density matrix formalism within a two-level approximation [26–28].

The organization of the paper is as follows: Section 1 contains the theoretical framework, in Section 2, we discussed the obtained results and, in Section 3, we report our conclusions.

1. Theoretical framework

The semiconductor MSQD $Al_{0.3}Ga_{0.7}As/GaAs/Al_{0.3}Ga_{0.7}As$ (Fig. 1) consisting of core $Al_{0.3}Ga_{0.7}As$, shell-well GaAs and outer shell $Al_{0.3}Ga_{0.7}As$ is under study. In order to investigate the effect of codirected external fields on the electron energy spectrum and wave functions, the Schrodinger equation is solved

$$H\Psi_{jm}(\vec{r}) = E_{jm}\Psi_{jm}(\vec{r}) \tag{1}$$

with the Hamiltonian

$$H = \left(\vec{p} - \frac{e}{c}\vec{A}\right)\frac{1}{2\ m(\vec{r})}\left(\vec{p} - \frac{e}{c}\vec{A}\right) + V_F(r,\theta) + U(r), \tag{2}$$

where $\vec{A}$ is the vector potential, $V_F(r,\theta) = -|e|F\ r\ \cos\ \theta$ is the electric field potential,

$$U(r) = \begin{cases} V_0, & 0 < r \le r_0,\ \ r_1 < r \le r_2 \\ 0, & r_0 < r \le r_1 \\ \infty, & r > r_2 \end{cases} \tag{3}$$

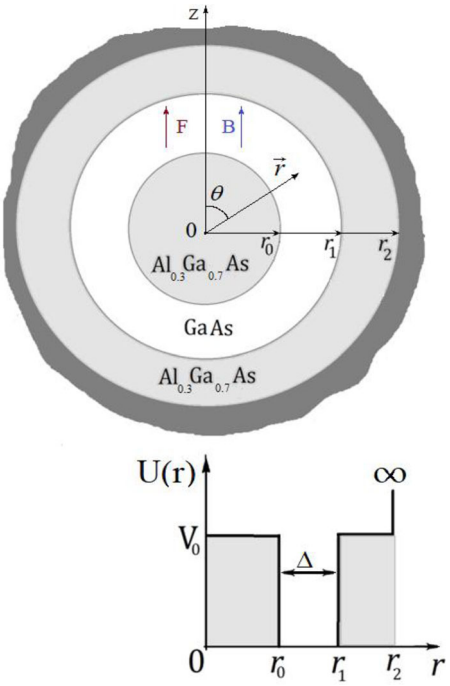

Figure 1. Geometric and potential scheme of QAD.

$$m(r) = \begin{cases} m_0, & 0 < r \le r_0, \ \ r_1 < r \le r_2 \\ m_1, & r_0 < r \le r_1 \end{cases} \tag{4}$$

confinement potential and electron effective masses. In order to solve the equation (1), the wave functions are expanded over the complete set of exact solution of Schrödinger equation for an electron in the same QAD without the external fields [19]

$$\Psi_{jm}(\overrightarrow{r}) = \sum_n \sum_l c_{nl}^{jm} \Phi_{nlm}(\overrightarrow{r}) \tag{5}$$

$$\Phi_{nlm}(r) = R_{nl}(r) Y_{lm}(\theta, \varphi). \tag{6}$$

Here, the radial functions $R_{nl}(r)$ are defined by Bessel functions:

$$R_{nl}(r) = \begin{cases} A_{nl}^{(0)} i_l\left(k_{nl}^{(0)} r\right), & E_{nl} < V_1 \\ A_{nl}^{(0)} j_l\left(k_{nl}^{(0)} r\right), & E_{nl} \ge V_1 \\ A_{nl}^{(1)} j_l\left(k_{nl}^{(1)} r\right) + B_{nl}^{(1)} n_l\left(k_{nl}^{(1)} r\right) & \\ A_{nl}^{(2)} i_l\left(k_{nl}^{(2)} r\right) + B_{nl}^{(2)} \kappa_l\left(k_{nl}^{(2)} r\right), & E_{nl} < V_2 \\ A_{nl}^{(2)} j_l\left(k_{nl}^{(2)} r\right) + B_{nl}^{(2)} n_l\left(k_{nl}^{(2)} r\right), & E_{nl} \ge V_2 \end{cases} \tag{7}$$

The electron energy spectrum and unknown coefficients are obtained on the basis of the Ben Daniel Duke boundary conditions and normality of radial function:

$$\left.\begin{aligned} R_{nl}^{(i)}(r_i) &= R_{nl}^{(i+1)}(r_i) \\ \frac{1}{m_i} \frac{dR_{nl}^{(i)}(r)}{dr}\bigg|_{r=r_i} &= \frac{1}{m_{i+1}} \frac{dR_{nl}^{(i+1)}(r)}{dr}\bigg|_{r=r_i} \end{aligned}\right\}, \ \ i = 0, 1 \tag{8}$$

$$\int_0^{r_2} |R_{nl}(r)|^2 r^2 dr = 1. \tag{9}$$

The expanded coefficients of the wave functions c_{nl}^{jm} and the energy spectrum E_{jm} are obtained from secular equation

$$\left| H_{nl,\,n'l'} - E_{jm} \delta_{n,\,n'} \delta_{l,\,l'} \right| = 0, \tag{10}$$

where, the matrix elements $H_{nl,\,n'l'}$ looks like

$$\begin{aligned} H_{n'l',\,nl} = \left(E_{nl}^0 + m\eta\right) \delta_{n',\,n} \delta_{l',\,l} - |e| F \left\{ \alpha_{l,\,m} \delta_{l',\,l+1} + \beta_{l,\,m} \delta_{l',\,l-1} \right\} I_{n'l',\,nl}^F + \\ \frac{1}{4} \eta^2 \left\{ \gamma_{l,\,m} \delta_{l',\,l+2} + \chi_{l,\,m} \delta_{l',\,l} + \lambda_{l,\,m} \delta_{l',\,l-2} \right\} I_{n'l',\,nl}^B \end{aligned} \tag{11}$$

$$I_{n'l',\,nl}^B = \int_0^{r_2} r^4 R_{n'l'}(r) R_{nl}(r) dr, \ \ I_{n'l',\,nl}^F = \int_0^{r_2} r^3 R_{n'l'}^*(r) R_{nl}(r) dr,$$

$$\alpha_{l,\,m} = -\sqrt{\frac{(l+1)^2 - m^2}{(2l+3)(2l+1)}}, \ \ \beta_{l,\,m} = -\sqrt{\frac{l^2 - m^2}{4l^2 - 1}},$$

$$\gamma_{l,\,m} = -\sqrt{\frac{[(l+2)^2 - m^2][(l+1)^2 - m^2]}{(2l+5)(2l+3)^2(2l+1)}},$$

$$\chi_{l,m} = 1 - \frac{(l+1)^2 - m^2}{(2l+1)(2l+3)} - \frac{l^2 - m^2}{4l^2 - 1}, \quad \lambda_{l,m} = -\sqrt{\frac{[(l-1)^2 - m^2](l^2 - m^2)}{(2l+1)(2l-1)^2(2l-3)}}.$$

The probability of intersubband quantum transitions is determined by the oscillator strength

$$F_{i-f} = 2m_1(E_i - E_f)\left|M_{if}\right|^2/\hbar^2, \tag{12}$$

where $M_{fi} = \langle \psi_i | er\cos\theta | \psi_f \rangle$ is a dipole transition matrix element (electromagnetic wave is polarized in the axial direction).

The expression for linear $\alpha^{(1)}(\omega)$, the third-order nonlinear $\alpha^{(3)}(I,\ \omega)$ and total absorption $\alpha(I,\ \omega)$ coefficients are written as follows, respectively

$$\alpha^{(1)}(\omega) = \sqrt{\frac{\mu}{\varepsilon_r}} \frac{\sigma_\nu\ \hbar\omega\ \Gamma_{fi}\left|M_{fi}\right|^2}{\left(E_{fi} - \hbar\omega\right)^2 + \left(\hbar\Gamma_{fi}\right)^2} \tag{13}$$

$$\alpha^{(3)}(I,\ \omega) = -\sqrt{\frac{\mu}{\varepsilon_r}}\left(\frac{I}{2\ n_r\ \varepsilon_0 c}\right) \frac{\sigma_s\ \hbar\omega\ \Gamma_{fi}\ \left|M_{fi}\right|^2}{\left[\left(E_{fi} - \hbar\omega\right)^2 + \left(\hbar\Gamma_{fi}\right)^2\right]^2} \times \left\{4\left|M_{fi}\right|^2 - \frac{(M_{ff} - M_{ii})^2\left[3E_{fi}^2 - 4E_{fi}^2\hbar\omega + \hbar^2\left(\omega^2 - \Gamma_{fi}^2\right)\right]}{E_{fi}{}^2 + \left(\hbar\Gamma_{fi}\right)^2}\right\} \tag{14}$$

$$\alpha(I,\ \omega) = \alpha^{(1)}(I,\ \omega) + \alpha^{(3)}(I,\ \omega), \tag{15}$$

where I is the incident optical intensity, $\hbar\omega$ is the incident photon energy, μ is the magnetic permeability of the system, $\varepsilon_r = \varepsilon_0\ n_r^2$ is the real part of permittivity, n_r^2 is the static component of the semiconductor refractive index, c and ε_0 are the light speed and the electrical permittivity in vacuum, σ_s is the electron density, $E_{fi} = E_f - E_i$ is the energy difference between final and initial energy levels, the non-diagonal matrix element Γ_{fi} is called the relaxation rate of the initial and final state and it is the inverse of the relaxation time T_{fi}.

2. Analysis and discussion of results

The computer calculations were performed for $Al_xGa_{1-x}As/GaAs/Al_xGa_{1-x}As$ nanostructure with following physical parameters: $x = 0.3$, $m_0 = (0.067 + 0.083x)\ m_e = 0.092\ m_e$, $m_1 = 0.067\ m_e$ (m_e – free electron mass), $V_0 = 0.6\ (1155x + 370\ x^2) = 227.9$ meV, $r_0 = 5(15)$ nm, $r_1 = 15(25)$ nm, $r_2 = 20(30)$ nm, $\varepsilon = 11.5$ is the average dielectric constant.

The dependence of the electron states energies with $m = 0$ on the applied electric field at the magnetic field inductions $B = 0$ T, $B = 15$ T, $B = 30$ T in the QAD with $r_0 = 5$ nm, $r_1 = 15$ nm and $r_2 = 20$ nm (a-c) and $r_0 = 15$ nm, $r_1 = 25$ nm and $r_2 = 30$ nm (d-f) is shown in Fig. 2. As we can see, the ground state energy shifts to lower energy region as the electric field strength increases. For QAD with a larger core, this shift is bigger. The excited state energies are initially slightly dependent on the electric field. Though, after a certain value of the electric field strength the electron energy decreases very drastically. The magnetic field shifts all energy levels to higher energy region. The magnetic

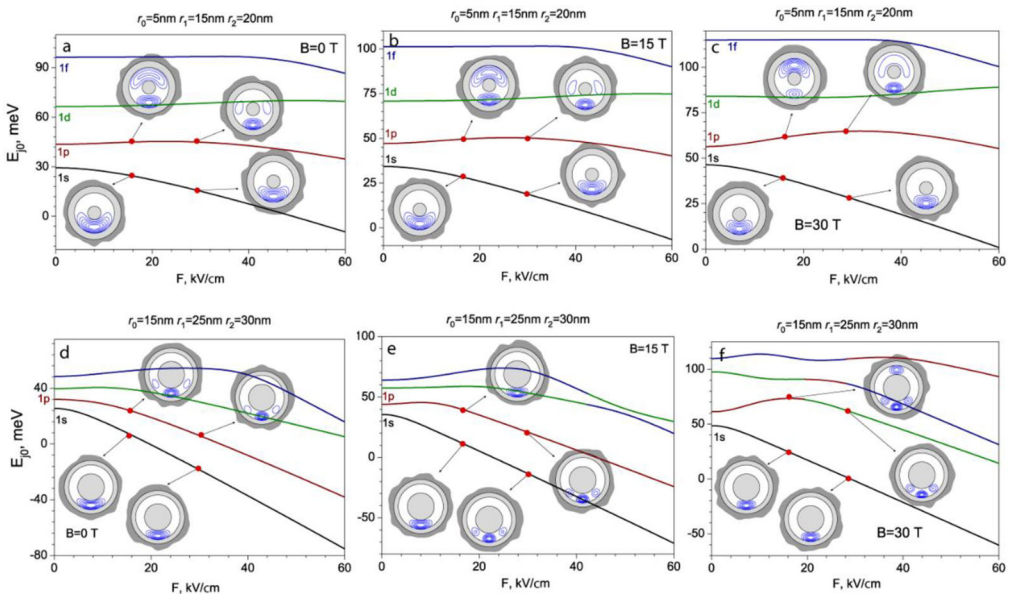

Figure 2. Dependence of the electron energy spectra on the applied electric field at $B = 0$ T, $B = 15$ T, $B = 30$ T in the QAD with $r_0 = 5$ nm, $r_1 = 15$ nm and $r_2 = 20$ nm (a–c) and $r_0 = 15$ nm, $r_1 = 25$ nm and $r_2 = 30$ nm (d–f).

field effect is stronger for a larger QAD. Different dependencies of energy levels on the electric and magnetic fields cause the energy level anticrossing.

The inserts in Fig. 2 show the electron density distribution in the nanosystem for the ground and first excited states. The electric field shifts electron density for 1 s state (ground state) in the direction opposite to the electric field strength. At the same time the electron density for the first excited state has two lobes and shifts in the same direction with the ground state only after a certain value of the electric field. The magnetic field compresses the electron density to the axial axis. For convenience, energy levels in the Fig. 2 are marked as 1 s, 1p, 1d, … according to the states with a certain value of the orbital quantum number, which predominates in the expansion of the respective wave functions. Due to the anticrossing effect, the order of the energy levels (1 s, 1p, 1d, 1f) changes. As it is shown in Fig. 2, more changes occur in order of the energy levels in case of QAD larger size and stronger magnetic field. The electron states of the different symmetry are shown in the figure by the corresponding colors (s – black, p – red, d – green, f – blue) in order to mark the change in the symmetry of the states when the electric field strength changes. For example, the electron energy level in the state with a symmetry close to 1p at the increasing electric field strength moves from the second ($j = 2$ at $F < 20$ kV/cm) to the fourth position ($j = 4$ at $F > 30$ kV/cm) due to anticrossing effects (Fig. 2f).

The magnetic field effect on the electron energy spectrum and charge distribution in QAD is stronger for larger QAD. Therefore, further calculations are performed only for larger QAD (r_0=15 nm, r_1=25 nm, r_2=30 nm). Fig. 3 shows the dependences of the oscillator forces for quantum transitions from the ground to the excited states 1-2, 1-3, 1-4 (solid lines), and transitions between the excited states 2-3 (dashed line) on the

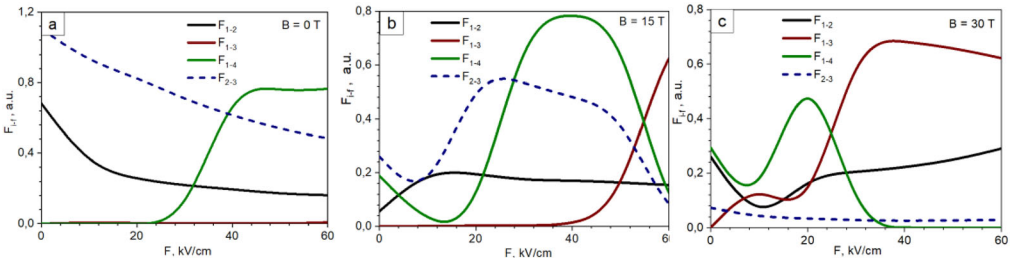

Figure 3. Dependence of the oscillator strength quantum transitions on the electric field at B = 0T (a), B = 15T (b), B = 30T (c) in the QAD r_0=15nm, r_1=25nm, r_2=30nm.

electric field strength at $B = 0$, 15, 30 T. At the magnetic field absence, the oscillator strength for allowed quantum transitions (1-2, 2-3) rapidly decreases with the increase of the electric field strength. Though, the oscillator strength for transition 1-3, which is forbidden by the selection rules for spherical systems, increases rapidly at $F > 30$ kV/cm. In the magnetic field presence, there is a nonmonotonic dependence of the oscillator forces with the increase of the electric field. The oscillator strength for allowed transition 1-2 is less than for transitions from the ground to more excited states (1-3, 1-4). This is a consequence of a significant violation of the spherical symmetry of the system. The new quantum states are a combination of states of the undisturbed system and the selection rules for spherical systems are not valid.

Fig. 4 demonstrates features of the joint influence of the electric and magnetic fields on the light absorption coefficient caused by different quantum transitions. The dependences of the linear (dotted), the third-order nonlinear (dotted) and total (continuous) optical absorption coefficients caused by quantum transitions: 1-2, 1-3, 2-3 on the energy of the incident photon are calculated. The colors indicate different values of the electric field ($F = 0$ – red, $F = 15$ kV/cm – green, $F = 30$ kV/cm – blue).

The height peak of the linear and nonlinear absorption coefficients caused by the quantum transition 1-2 increases with the increasing magnetic field at $F = 0$. The value of the total absorption coefficient at low energies of the incident light becomes negative due to the shift of the nonlinear absorption peak to the low energy region. In the cases $F = 15$ kV/cm and $F = 30$ kV/cm, the absorption coefficient caused by the quantum transition 1-2 decreases with the increasing magnetic field. The value of the absorption coefficient caused by the quantum transition 1-3 at $B = 0$ or $B = 15$ T, as expected, is small and increases only at $B = 30$ T and $F = 30$ kV/cm. This is clear, since the oscillator strength $F_{1\text{-}3}$ increases rapidly under the simultaneous influence of the strong electric and magnetic fields. The electric field shifts the energy of quantum transitions to the region of higher energies, and only for the transition 2-3 at $B = 30$ T the opposite effect occurs.

These results are in good agreement with the results of studies of the electric and magnetic fields individual effects on the intersubband quantum transitions in spherical QDs [19–21, 26–28].

3. Conclusions

In this study, we have investigated the electron energy spectrum, electron density distributions in semiconductor QAD, oscillator strengths of the quantum transitions and

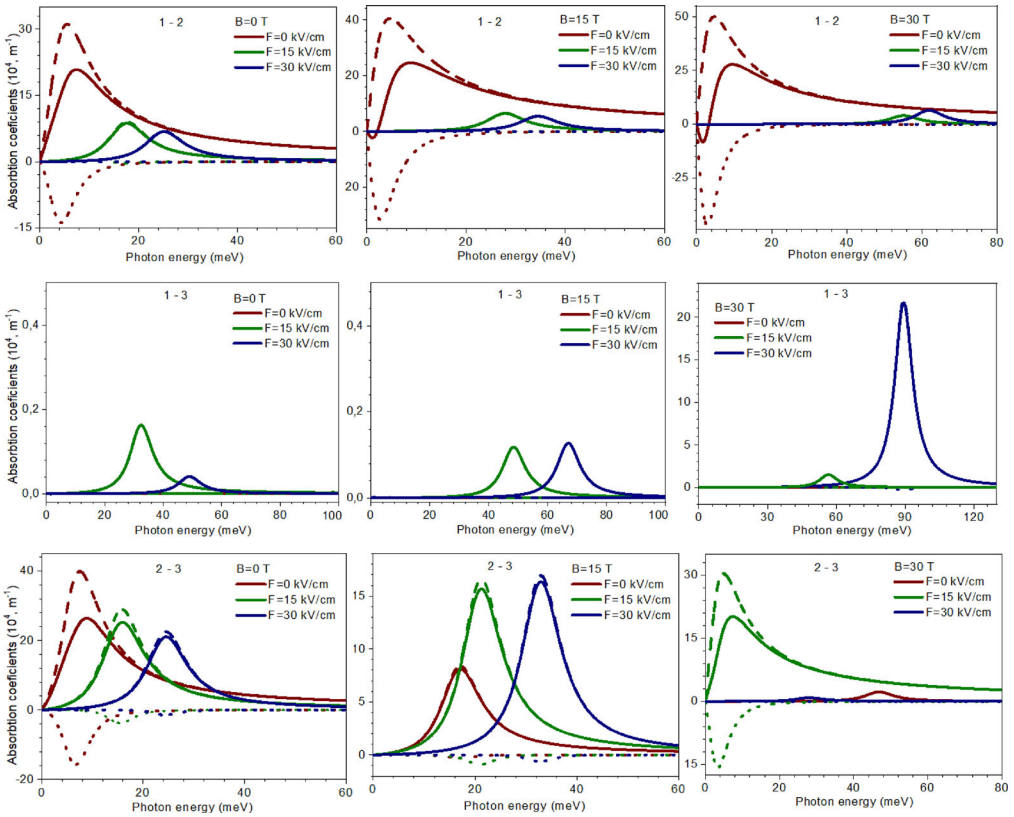

Figure 4. The linear (dashed), the third-order nonlinear (dotted) and total (solid) optical absorption coefficients of the QAD versus the incident photon energy $\hbar\omega$ with intensity $I = 0.04\,\mathrm{MW/cm^2}$.

optical absorption coefficient under the external electric and magnetic fields. The effective mass approximation and the model of finite rectangular potential barriers are used. It is found that the oscillator strengths of quantum transitions and OACs are strongly influenced by the magnetic field induction, electric field strength and a dot size. However, each parameter leads to different behavior of the OACs for each transition. It is shown that an increase in the electric field strength at different values of the magnetic field induction entails a different shift in the electron energy levels, which leads to level anticrossing. This is reflected in the oscillator strengths of intersubband quantum transitions, as well as in the height and position of the absorption coefficient peaks. The absorption coefficient peaks shift to the region of higher energies at the increase of the electric field strength.

ORCID

V. A. Holovatsky http://orcid.org/0000-0002-5573-2562

References

[1] D. Vasudevan *et al.*, *J. Alloy. Compd* **636**, 395 (2015). doi:10.1016/j.jallcom.2015.02.102
[2] C. Yan *et al.*, *Nanomaterials* **9** (8), 1100 (2019). doi:10.3390/nano9081100

[3] M. F. Frasco, and N. Chaniotakis, *Sensors (Basel)* **9** (9), 7266 (2009). doi:10.3390/s90907266
[4] G. S. Selopal *et al.*, *Adv. Funct. Mater* **30** (13), 1908762 (2020). doi:10.1002/adfm.201908762
[5] X. Wang, H. Li, and G. Chen, Core–shell nanoparticles for cancer imaging and therapy, in *Core–Shell Nanostructures for Drug Delivery and Theranostics* (Elsevier, Ámsterdam, 2018). doi:10.1016/B978-0-08-102198-9.00006-5
[6] G. Rudko *et al.*, *Nanoscale Res. Lett.* **11** (1), 83 (2016). doi:10.1186/s11671-016-1300-5
[7] M. J. Karimi, and G. Rezaei, *Phys. B Condens. Matter.* **406** (23), 4423 (2011). doi:10.1016/j.physb.2011.08.105
[8] B. Li *et al.*, *Phys. Lett. A* **372** (8), 1337 (2008). doi:10.1016/j.physleta.2007.09.075
[9] Z. H. Zhang *et al.*, *Superlattices Microstruct* **47** (2), 325 (2010). doi:10.1016/j.spmi.2009.12.004
[10] V. A. Harutyunyan, *Appl. Nanosci.* **2** (3), 339 (2012). doi:10.1007/s13204-012-0087-7
[11] D. A. Baghdasaryan, D. B. Hayrapetyan, and V. A. Harutyunyan, *Phys. B Condens. Matter.* **510**, 33 (2017). doi:10.1016/j.physb.2017.01.017
[12] A. Chafai *et al.*, *Mater. Devices* **3**, 1 (2018). doi:10.23647/ca.md20180504
[13] A. Boda, *Phys. B Condens. Matter* **575, 7**, 411699 (2019). doi:10.1016/j.physb.2019.411699
[14] E. C. Niculescu, and M. Cristea, *UPB Sci. Bull. Ser. A Appl. Math. Phys* **75** (2), 195 (2013).
[15] B. Çakır, Y. Yakar, and A. Özmen, *Phys. B Condens. Matter.* **510** (1), 86 (2017). doi:10.1016/j.physb.2017.01.018
[16] B. Çakır *et al.*, *Chem. Phys.* **475**, 61 (2016). doi:10.1016/j.chemphys.2016.06.010
[17] L. Stevanović, N. Filipović, and V. Pavlović, *Opt. Mater* **91** (11), 62 (2019). doi:10.1016/j.optmat.2019.02.049
[18] L. Stevanović, N. Filipović, and V. Pavlović, *Opt. Quantum Electron.* **48**, 4 (2016). doi:10.1007/s11082-016-0502-5
[19] V. Holovatsky, M. Chubrey, and O. Voitsekhivska, *Superlattices Microstruct.* **145**, 106642 (2020). doi:10.1016/j.spmi.2020.106642
[20] V. A. Holovatsky, M. Y. Yakhnevych, and O. M. Voitsekhivska, *Condens. Matter Phys.* **21**, 1 (2018). doi:10.5488/CMP.21.13703
[21] R. Kostić, and D. Stojanović, *J. Nanophoton* **6** (1), 061606–1 (2012). doi:10.1117/1.JNP.6.061606
[22] M. H. Tanhaei, and G. Rezaei, *Superlattices Microstruct* **98**, 29 (2016). doi:10.1016/j.spmi.2016.08.001
[23] V. A. Holovatsky, O. M. Voitsekhivska, and M. Y. Yakhnevych, *Physica E* **93**, 295 (2017). doi:10.1016/j.physe.2017.06.019
[24] V. Holovatsky, I. Bernik, and M. Yakhnevych, *Physica E* **83** (9), 256 (2016). doi:10.1016/j.physe.2016.04.035
[25] M. V. Chubrei, V. A. Holovatsky, and C. A. Duque, *Philos. Mag* **101** (24), 2614 (2021). doi:10.1080/14786435.2021.1979267
[26] E. B. Al *et al.*, *Physica E* **119**, 114011 (2020). doi:10.1016/j.physe.2020.114011
[27] E. B. Al *et al.*, *Philos. Mag* **101** (1), 117 (2021). doi:10.1080/14786435.2020.1821112
[28] E. B. Al *et al.*, *Phys. B Condens. Matter* **613**, 412874 (2021). doi:10.1016/j.physb.2021.412874